TIME-ACCURATE SIMULATION OF THE FLOW AROUND THE COMPLETE BO105 WIND TUNNEL MODEL

Walid Khier, Thorsten Schwarz, Jochen Raddatz

Institute of Aerodynamics and Flow Technology,
German Aerospace Center (DLR)
Member of the Helmholz Association

Lilienthalplatz 7, 38108 Braunschweig - Germany

Abstract

Air flow past a reduced scale model of an Eurocopter BO-105 fuselage-main rotor-tail rotor configuration was simulated by solving the time dependent Navier-Stokes equations. The computations correspond to wind tunnel measurements carried out under Mach 0.1578 forward flight conditions. Main and tail rotors' blades were considered rigid in the computations, and their motions by were achieved by a moving overlapping grid technique (Chimera). The numerical results are judged against unsteady pressure measured on the fuselage and the blades. Apart from blade elasticity effects, good agreement with experiment was found.

List of Symbols

M_∞	Free stream Mach number
M_{MR}	Main rotor tip Mach number
M_{TR}	Tail rotor tip Mach number
Ψ	Azimuth angle
Θ_{MR}	Main rotor pitch angle
Θ_{TR}	Tail rotor pitch angle
C	Chord length
C_p	Pressure coefficient

Introduction

Helicopters operate under a wide range of flying conditions, and hence, significantly different flow patterns develop around them. As a result, strong unsteady interactional phenomena take place, such as blade-vortex interaction, especially during descend flight, or tail shake under certain forward flight conditions.

Although helicopter flows are highly unsteady, emphasis was placed so far by aerodynamicist mainly on the time averaged characteristics of the flow rather than its unsteady aspects. However, proper understanding of the flow around helicopters requires thorough analysis of its time dependant behaviour. In addition, an ever growing awareness of environmental issues has evolved over the past three decades, which resulted in strict noise emission regulations. As a result, special attention has been directed lately to the acoustic performance of helicopters, and therefore, advanced analysis of the unsteady aspects of helicopter aerodynamics is needed.

From the view point of CFD, simulation of complete helicopter poses a serious challenge, not only because of the complex flow physics, but due to the wide range of Mach numbers and flow regimes involved as well. The flow around the bluff fuselage is incompressible and characterized by three dimensional separation. The blades, on the other hand, encounter significantly different flows. In forward flight transonic, and partially supersonic, flow with shocks is found on the tip of the advancing blade, and low speed reversed flow near the roots of the retreating blades. Time accuracy is another issue increases the severity of the problem. Proper resolution of the rotor motion and the resulting flow phenomena limits the time steps drastically, and thus require considerable computational resources.

These intensive computer requirements were mainly the reason why many recent research considered individual elements of the helicopter for time-accurate calculations (Refs. [1-5]) or limited the number of grid points used as in Refs. [7-8], or were limited to the solution of Euler equations only (Ref [9]).

Therefore, numerical simulation of helicopter fuselage-main rotor-tail rotor configuration was

defined as a final milestone of the DLR-ONERA co-operation project CHANCE [10-11]. The numerical approach is based on the solution of the time-accurate Reynolds (Favre) averaged Navier-Stokes equations in three dimensions using finite volume formulation and Chimera overlapping grid technique. Overlapping grids method, Ref [12], was used in the present computations because of the following reasons. Firstly, compared to alternative approaches (re-meshing for example), relative motion between the different components of the helicopter can be easily realized. Secondly, Chimera reduces the time and effort required to generate block structured grids around complex configurations like that of a helicopter. Moreover, overlapping grids allow modular construction of nearly any complex configuration, and thus, the contribution of the various components of the aircraft to its aerodynamic characteristics can be relatively easily studied.

The reported work is an intermediate step towards the time-accurate simulation of a complete helicopter, including engine intake and exhaust, detailed rotors with hubs taking the elastic deformation of blades into account. In this paper a preliminary validation of the DLR's simulation code FLOWer to predict time-dependent flow fields around a fuselage-main rotor-tail rotor configuration based on rigid blade assumption is presented. The prediction ability of FLOWer is demonstrated by time-accurate computations of the flow past a powered reduced scale wind tunnel model of the Eurocopter BO-105 helicopter.

The next part of the paper describes the simulated geometry and flow conditions. The numerical approach and computational grid are presented in the subsequent parts. The fifth part discusses the numerical results and compares them with experimental data, and the conclusions drawn therefrom are given in the last section of this paper.

Simulated test case and flow conditions

The computations reported here simulates a forward flight measured in the HeliNOVI test campaign [13-14]. Figure 1 shows the model mounted on a model support inside the German-Dutch wind tunnel (*DNW*). The tests were carried out on a 1:2.5 scale model of an EuroCopter BO-105 with a main rotor diameter of 4 m and a tail rotor diameter equal to 0.773 m. Both the main and tail rotors have square blades. The main rotor blades consist of -8° linearly twisted NACA 23012 profile, and chord length equal to 0.121 m, while the tail rotor is made of MBB S 102 E airfoil with zero twist, and has a chord length equal to 0.0733 m. The experimental model, its instrumentation and the wind tunnel tests are described in detail by Ref [15].

All intake and ventilation openings were closed in the experimental model. Surface details like antennas, windscreen wipers, door handles,... etc. were omitted. A cylindrical strut was used to support the model in the wind tunnel. The computational model was constructed from a three dimensional scan of the fuselage of the experimental model, and the surfaces of the blades, the horizontal stabilizer and end plates were constructed from airfoil data. The model strut, spoiler and landing skids were retained in the computations. Rotors' hubs and drive shafts were not considered at this step, and the rotors were represented by disconnected rigid blades (Figure 1 right).

The selected test case refers to a forward flight at angle of attack equal to –5.2°. The main and tail rotor angular velocities are equal to 1085 and 5304 *RPM,* respectively, corresponding to main rotor tip Mach number, M_{MR} equal to 0.652, and tail rotor tip Mach number, M_{TR} equal to 0.63. The test was carried out with a free stream velocity equal to 60 m/s (M_∞=0.1766). The rotors were not trimmed numerically, rather both the main and tail rotor blade pitch angles were specified according to the nominal trim law used in experiment, that is Θ_{MR} = 10.5°-6.3°sin(Ψ)+1.9°cos(Ψ) for the main rotor, and Θ_{TR}=8° for the tail rotor, where Ψ is the main rotor's azimuth angle, and Θ_{MR} and Θ_{TR} main and tail rotor pitch angles, respectively.

Numerical Approach

Description of the solver

The Reynolds (Favre) averaged Navier-Stokes equations were solved by means of the CFD simulation code FLOWer. The solution process follows the idea of Jameson, Ref [16], which represents the mass, momentum and energy fluxes by a second order central differences. Third order numerical dissipation is added to the convective fluxes to ensure numerical stability. These dissipative contributions are reduced to first order when a shock is detected. Smooth transition from the fourth to the second order is realized by linear combination of both terms.

FLOWer contains a large array of statistical turbulence models, ranging from algebraic and one-equation eddy viscosity models (Refs [17-18]) to seven-equation Reynolds stress model. In this paper

a slightly modified version of Wilcox's two-equation k-ω model is used. The modifications, their validation and implementation are given in Ref [19], while Ref [20] describes the original model of Wilcox. Unlike the main flow equations, Roe's scheme is employed to compute the turbulent convective fluxes.

The descretized equations are advanced in a fictitious time using a explicit multi-stage Runge-Kutta method. The solution process makes use of acceleration techniques like local time stepping, multigrid and implicit residual smoothing. Turbulence transport equations are integrated over pseudo-time implicitly. Each (pseudo) time step, a system of equations is solved by the DDADI (diagonal dominant alternating direction implicit) to obtain k- and ω. No assumptions are made for the boundary layer profile, rather, the equations of motion are integrated down to the wall (*Low-Re* approach). One particular advantage of the k-ω class of models is the automatic damping of the turbulence kinetic energy in the laminar sublayer, which removes the need of explicit damping functions thus making the Low-Re approach particularly interesting, despite the required fine resolution of the near wall region .

Flow data is exchanged between Chimera components and/or background by interpolation on the outer boundaries of each child grid. At the same time, solid bodies contained in the child grid blank all points those lie inside the solid surface creating a "hole" in the other grids. These points are ignored in the solution procedure, and only the points on the hole boundaries are updated by interpolating the flow variables from the child (embedded) grids. The details of the procedure are given in [12].

Computational grid

The configuration has been subdivided into 12 components: fuselage, horizontal stabilizer and end plates (left and right), four main rotor blades, two tail rotor blades, left and right skids, and model strut+spoiler. Multi-block structured grids were generated around each component. The twelve components were embedded in a locally refined Cartesian background grid consisting of 414 blocks containing 1.9 Million cells. Table 1 contains an overview of the components grids.

	No. of points	No.of blocks
Fuselage	2.310.000	17
MR Blade grid (x4)	840.000	3
TR Blade grid (x2)	350.000	2
Skid (x2)	675.000	6
Stabilizer grid (x2)	770.000	5
Strut+Spoiler	1.090.000	6
Background grid	2.240.000	414
Total	12.560.000	477

Table 1: Overview of the numerical grid

Figure 2 shows the numerical grid on the surface of the helicopter together with a cross section in the background grid. The figure shows also the near field grids around the different components of the aircraft.

Results and Discussion

A snapshot of the computed vortex structure is shown in Figure 3 in terms of constant λ_2 surfaces. The figure illustrates an extremely complex flow field with several interacting vortex systems. Evident blade-tip vortex interaction, and also between the wakes of the main rotor blades and the engine intake fairing can be seen. Although difficult to identify from the figure, vortices shed from main rotor blade roots could be preserved by the grid long enough to interact with two successive blades. The computations could reproduce the interaction of the main rotor wake with the tail rotor, which is typical for this advance ratio. Clearly observed also is unsteady vortex shedding from the helicopter skids and the model support.

Pressure distribution on the fuselage

A total number of 13 transducers were placed on the symmetry plane to measure air pressure variations with main rotor's azimuth position. Figure 4 shows a comparison of numerical and measured pressures along the centreline of the fuselage for the azimuth range between two identical constellations of the rotors (180^o main rotor or 900^o tail rotor) at a resolution of 30 main rotor degrees. The pressure patterns are qualitatively similar showing stagnation of the flow on the front end of the fuselage followed by acceleration marked by pressure reduction over the upper surface. A gradual increase in pressure is observed around x=-0.15 indicating deceleration of the flow. The stagnation pressure is reached again in front of the closed engine intake followed by a sharp suction peak over its upper leading edge. The pressure remains more or less constant over the engine intake and increases rapidly between x=0.7 and x=1.1, and continues to increase but at a slower, nearly linear rate until the tail fin is reached (around x=2.3). On the lower side the pressure decreases first over the nose reaching the lowest value close to x=-0.5, then increases with the distance between x=-0.5 and x=-0.3 where the pressure increase starts to be less steep. The blockage effect of the strut is indicated by a visible rise in pressure (x=0.52). The

pressure decreases then slowly over the lower side of the tail boom.

Unsteady effects are rather weak on the front part of the fuselage except for higher pressure in the engine intake area at $\Psi=60^o$ and over the upper side for the $\Psi=180^o$ position. The unsteadiness is most obvious in the tail boom area. Both qualitative and quantitative differences can be clearly seen. There is a noticeable pressure increase on the upper side caused most probably by the downwash of the main rotor blades when they pass over the tail boom ($\Psi=90^o$ and 180^o). Also observed are pressure pulsation propagating upstream as a result of the tail rotor motion. They are however damped quickly and become insignificant upstream of x=1.5.

Compared to the experiment, the computed pressure is very well predicted over the front part of the fuselage. The quality of predictions varies strongly on the tail boom and the tail fin with the azimuth position. While the numerical values remains acceptable in magnitude, there is what looks like a phase shift between the computed results and experiment. The deviations appears to be systematic on the tail boom where a higher pressure is predicted whenever the main rotor blades become parallel to the tail boom ($\Psi=90^o$ and 180^o).

The tail fin pressures are best examined in Figure 5, which illustrates the computed and measured instantaneous pressure signals for two locations on the tail fin. Apart from few exceptions, the computations underestimate the (ordinate direction opposite to Figure 5), but shows a similar behaviour to the experiment where five suction peaks corresponding to the tail rotor blades can be observed in both cases. However, as far as the azimuth position is concerned, the peaks are predicted earlier by the computations than the experiment. It is interesting also to notice the higher pressure levels recorded by the upper sensor, which is possibly caused by interaction between the rotor hub's wake and the tail fin; and therefore, not visible in the numerical results.

Main rotor pressure

Unsteady pressures on the main rotor were obtained at the radial position r/R=0.87 from two different blades by 20 dynamic pressure sensors. Signals from 15 sensors provided the unsteady pressure for the first blade, 10 on the upper side and 5 on the lower side; pressure data for the second blade was provided by 3 sensors on the upper side and 2 on the lower side. The numerical and experimental pressures normalized by the speed of sound (C_pM^2) are compared in Figure 6. Very good agreement between the numerical data and the experiment can be found, except for the azimuth positions between 120^o and 180^o. Within this range the computations show lower pressures and steeper adverse pressure gradients on the upper surface which are not observed in the experiment. On the pressure side the measured pressure is lower than the computed one indicating smaller effective pitch angle most probably due to elastic deformation of the blades similar to the observations of Pahlke [3].

Tail rotor pressure

The distributions of tail rotor pressures are shown for the radial position r/R=0.8 in
Figure 7 in terms of the C_pM^2. The advancing blade ($-90^o \le \Psi_{TR} \le 90^o$) generates higher thrust than the experimental one as can be deduced from the pressure pattern on the upper and lower sides of the blade. The smooth pressure recovery on the suction side steepens clearly around $\Psi=30^o$ and possibly becomes a shock in the tip region. However, this effect, which is completely absent in the experiment, vanishes rapidly and is hardly noticed for the $\Psi=60^o$ position. An opposite trend is observed for the retreating blade ($90^o \le \Psi_{TR} \le 270^o$) where smaller pressure differences between the pressure and suction sides are observed in the numerical results than in the experiment. An alternative view is provided the pressure time history given by Figure 8. The figure shows the evolution of pressure in time at two radial positions, r/R=0.5 and r/R=0.8. From the figure it can be clearly seen that computed pressure is insensitive to the radial position compared to the measured one. An alternating pressure pattern can be seen for the experimental data where the pressure coefficient rises rapidly from –0.36 to 0.1 at r/R=0.5, and from –0.74 to 0.15 at r/R=0.8. The pressure falls again forming a weak suction peak with a pressure coefficient value around –0.1 and –0.2 for the r/R=0.5 and 0.8 respectively. This suction peak is also seen in the numerical results but with a larger amplitude –0.4 and –0.55 for the same positions. The positive pressure pulse observed in the experiment can be hardly seen in the CFD results for the r/R=0.5 position. For the r/R=0.8 location there is a pressure recovery following the negative pressure peaks but it does not exceed -0.1, and always ahead of the experiment.

Since the measurements did not provide any information on the flapping of the tail rotor blades (due to flapping sensor damage), it was difficult to asses the importance of the flapping motion, and

therefore, was not considered in the simulation. In an attempt to verify these differences, a rotor simulation code [21] was applied to trim the rotor according to the measured thrust. The simulation resulted in a 41% reduction of the collective pitch due to the flap-pitch coupling, and cyclic components as high as 39% of the nominal pitch used in the computations. Recent HeliNOVI measurements confirmed these findings showing a deviation in collective pitch in the order of $\pm 2.5^{o}$. One possible and very probable reason for the observed deviation therefore may be this incompatibility in the tail rotor's control angles. However, a conclusive comment can not be made without re-computing the flow with the new trim.

Summary and conclusions

A Time-accurate Navier-Stokes simulation of a powered wind tunnel model of a BO-105 helicopter has been presented. The computations considered forward flight conditions at 60 m/sec and -5.2^{o} angle of attack. Main and tail rotor motions were realized numerically by a moving Chimera method with a resolution of 0.4^{o} and 2^{o} respectively. Periodic solutions were obtained in 700 hours elapsed time using 8 NEC-SX6 processors (5600 CPU hours), and needed 0.4 TB to store the results. More details on the performance can be found in [12]. The outcome of this work can be summarized as follows:

Despite the intensive computer and human resources demands involved, time-accurate simulation of complete helicopter is possible with the available CFD techniques.

The reported computations provided important guidelines for CFD development work at DLR. Additional tests (not reported here) revealed an order of magnitude acceleration in Chimera search operations, which means a speed up of 250% of the overall performance of FLOWer. The latest bench mark tests using a NEC-SX8 shows a speed up of 700%.

Very good agreement with experiment could be obtained for the fuselage. The largest deviations were observed when the main rotor blades crossed the tailboom.

Noticeable differences between the CFD results and experiment were found on the tail rotor. This was due to significant deviation in rotor's pitch and flap angles from the nominal trim law which was used in the computations.

Main rotor pressure could be predicted satisfactorily. As expected, some deviation from the experimental results was observed on the advancing blade due to blade elasticity.

The reported efforts are an important step towards the simulation of complete helicopters. To achieve this goal, the aforementioned elastic deformation and rotors' hubs effects will be verified within the EU-project GOAHEAD by wind tunnel measurements planned and dedicated for validation of CFD results.

Acknowledgments

This work was supported by *Bundes Ministerium für Bildung und Forschung* and *Bundes Ministerium für Wirtschaft und Arbeit*. The authors would also like to thank Dr. Yanping Yin and Mr. Hans-Jürgen Langer of DLR for providing the experimental data.

References

1. P. Beaumier, E. Chelli, K. Pahlke, Navier-Stokes Prediction of Helicopter Rotor Performance in Hover Including Aero-Elastic Effects, American Helicopter Society 56th Annual Forum, Virginia Beach, Virginia, May 2-4, 2000.

2. E. Chelli, K. Pahlke, Calculation of Viscous Flow Around the BO105 Main Rotor in Hover, DLR Internal Report IB-NR 129-99/27.

3. K. Pahlke, B. van der Wall, Calculation of Multibladed Rotors in High-Speed Forward Flight with Weak Fluid-Structure-Interaction, 27th European Rotorcraft Forum, 11-14 September 2001, Moscow, Russia.

4. H. Pomin, S. Wagner, Navier-Stokes Analysis of Helicopter Rotor Aerodynamics in Hover and Forward Flight, AIAA Paper 2001-0998.

5. H. Pomin, S. Wagner: Aeroelastic Analysis of Helicopter Rotor Blades on Deformable Chimera Grids, AIAA Paper 2002-0951.

6. H. v. Geyr, N. Kroll, Application of 3D-Preconditioning for the Prediction of Helicopter Fuselage Drag Considering Interferences with Model Support Strut}, 25 th European Rotorcraft Forum, 14-16 September 1999, Rome, Italy.

7. W. Khier, F. le Chuiton, T. Schwarz, Navier-Stokes Analysis of the Helicopter Rotor-

Fuselage Interference in Forward Flight, CEAS Aerospace Aerodynamics Research Conference, 10-12 June 2002, Cambridge, England.

8. T. Renauld, Unsteady Simulations of Complete Helicopters with the elsA Software, ONERA internal report No. RT 2/07783 DAAP-January 2005.

9. T. Schwarz, Berechnung der Umstroemung einer Hubschrauber-Rotor-Rumpf-Konfiguration auf der Basis der Euler-Gleichungen mit der Chimaeren-Technik, DLR Internal Report IB-NR 129-97/23.

10. K. Pahlke, M. Costes, A. D'Alascio, C. Castellin, A. Altmikus, Overview of Results Obtained During the 6-Year French-German Chance Project. 31st European Rotorcraft Forum, 13-15 September 2005, Florence, Italy.

11. J. Sides, K. Pahlke, M. Costes, Numerical Simulation of Flows Around Helicopters at DLR and ONERA. Aerospace Science and Technology, Vol. 5, pp 35-53, 2001.

12. T. Schwarz, The Overlapping Grid Technique for the Time-accurate Simulation of Rotorcraft Flows. 31st European Rotorcraft Forum, 13-15 September 2005, Florence, Italy.

13. H.-J. Langer, B Junker, V, Plassmeier, F Buchner, V. Mikulla, E. Mercker, The Unique Capabilities of a Complete Mach-Scaled Helicopter Model for the DNW-LLF, 27th European Rotorcraft Forum, Sept.11-14, 2001; Moscow, Russia

14. H.-J. Langer, O.Dieterich, S.Oerlemans, O. Schneider, B. v.d. Wall, J.Yin, The EU HeliNOVI Project -Wind Tunnel Investigations for Noise and Vibration Reduction. 31st European Rotorcraft Forum, 13-15 September 2005, Florence, Italy.

15. Jianping Yin, Berend Van der Wall, Stefan Oerlemans et al., Representative Test results from HeliNOVI Aeroacoustic Main Rotor/Tail Rotor/Fuselage Test in DNW. 31st European Rotorcraft Forum, 13-15 September 2005, Florence, Italy.

16. A. Jameson, W. Schmidt, E. Turkel, Numerical Solutions of the Euler Equations by Finite Volume Methods using Runge-Kutta Time-Stepping Schemes, AIAA-Paper 81-1259, 1981.

17. B. S. Baldwin, H. Lomax, Thin Layeer Approximation and Algebraic Model for Separated Turbulent Flows, 78-0257, 1978.

18. P. R. Spalart, S. R. Allmaras, A One-Equation Turbulence Model for Aerodynamic Flows, AIAA paper, 92-439, 1992.

19. R. Rudnik, Untersuchung der Leistungsfähigkeit von Zweigleichungs-Turbulenzmodellen bei Profilumströmungen, Deutsches Zentrum für Luft- und Raumfahrt e.V., FB 97-49

20. D. C. Wilcox, Reassessment of the Scale-Determining Equation for Advanced Turbulence Models, AIAA Journal, vol. 26, no. 11, November 1988.

21. Jianping Yin, Institute of Aerodynamics and Flow Technology, German Aerospace Center (DLR), private communications.

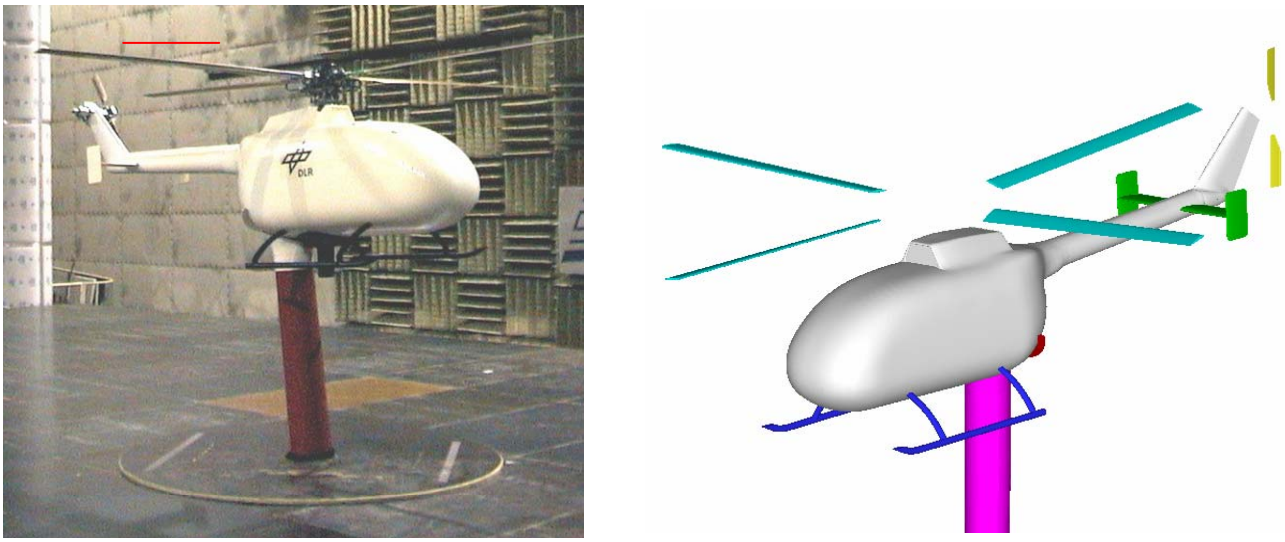

Figure 1: Left:BO-105 wind tunnel model and experimental setup, right:The CFD model

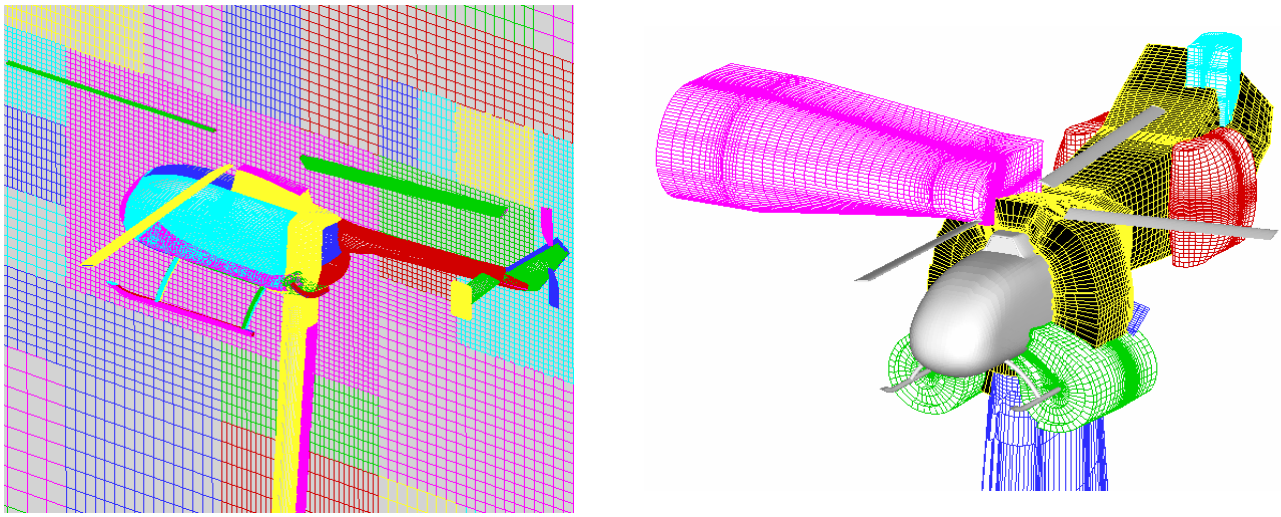

Figure 2: Left:surface grid and a cross section in the background grid, right:component (child) grids around the individual elements of the configuration

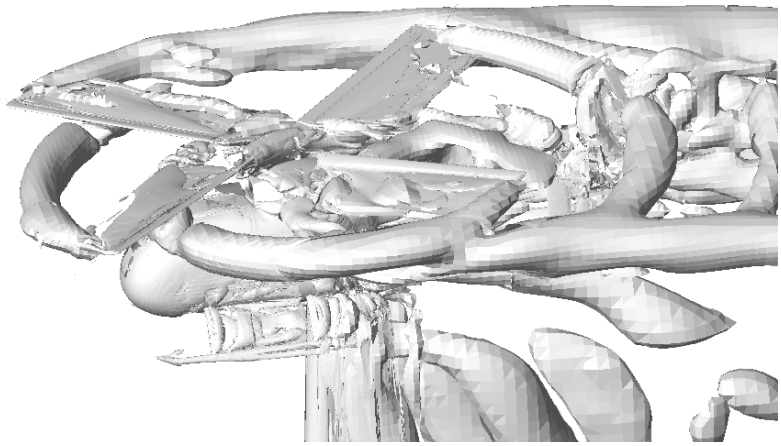

Figure 3: Computed instantaneous constant λ_2 surfaces

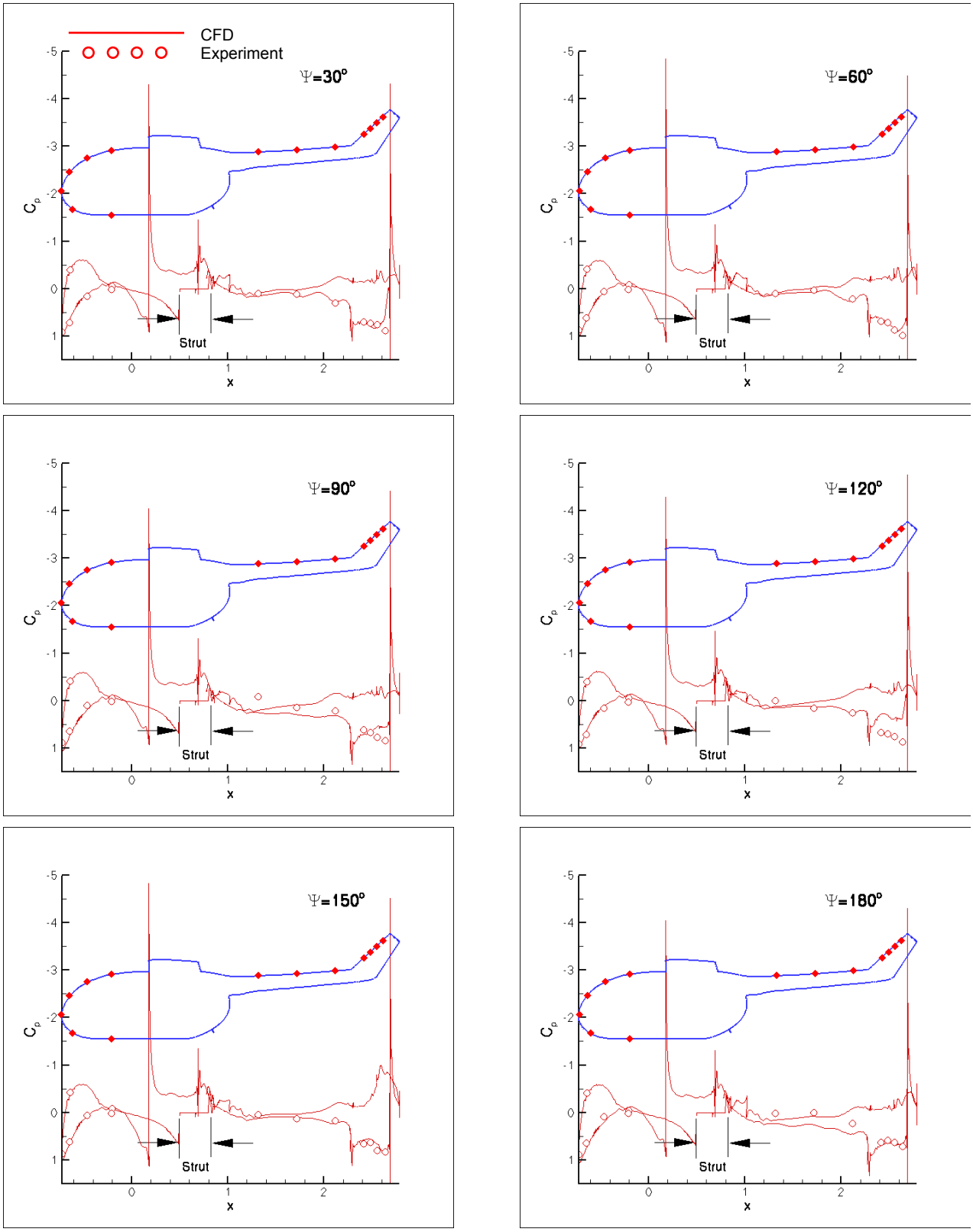

Figure 4: Comparison of computed (lines) and measured (symbols) pressure on the fuselage at symmetry plane for different main rotor azimuth angles

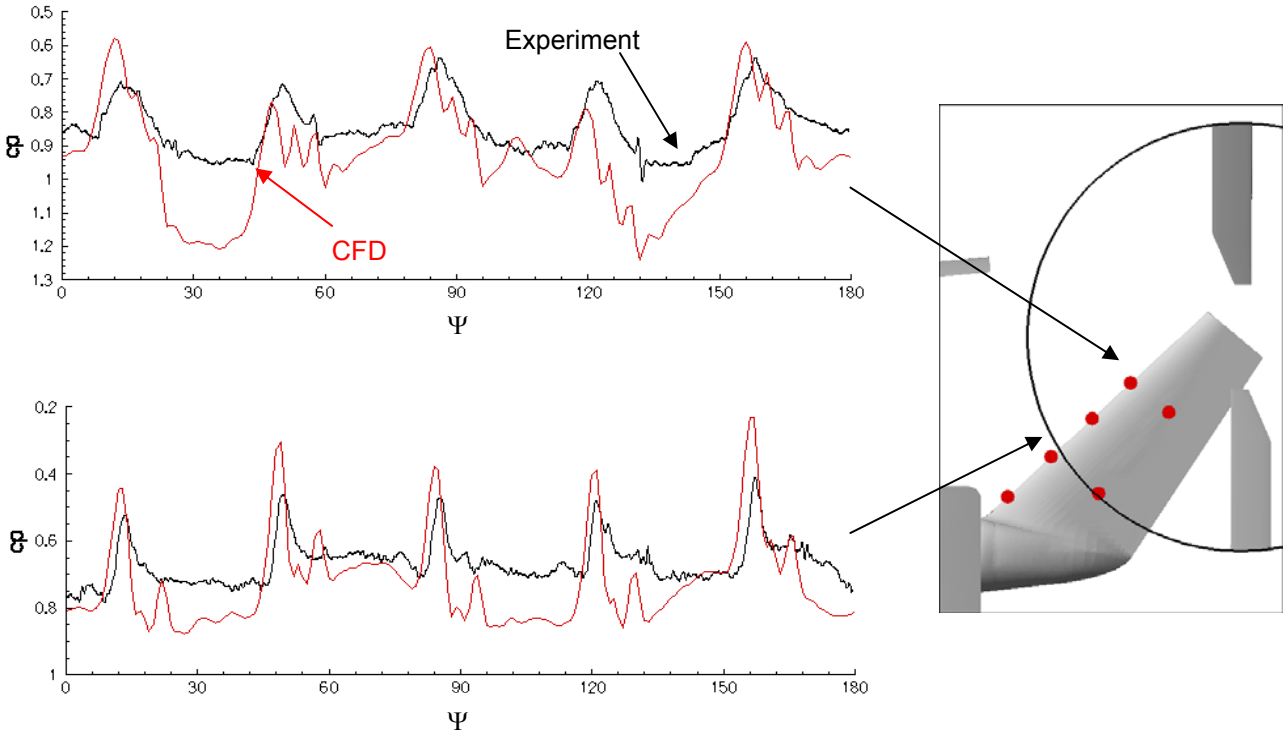

Figure 5: Computed (red) and measured (black) unsteady pressure coefficients on the tail fin as a function of the main rotor azimuth position

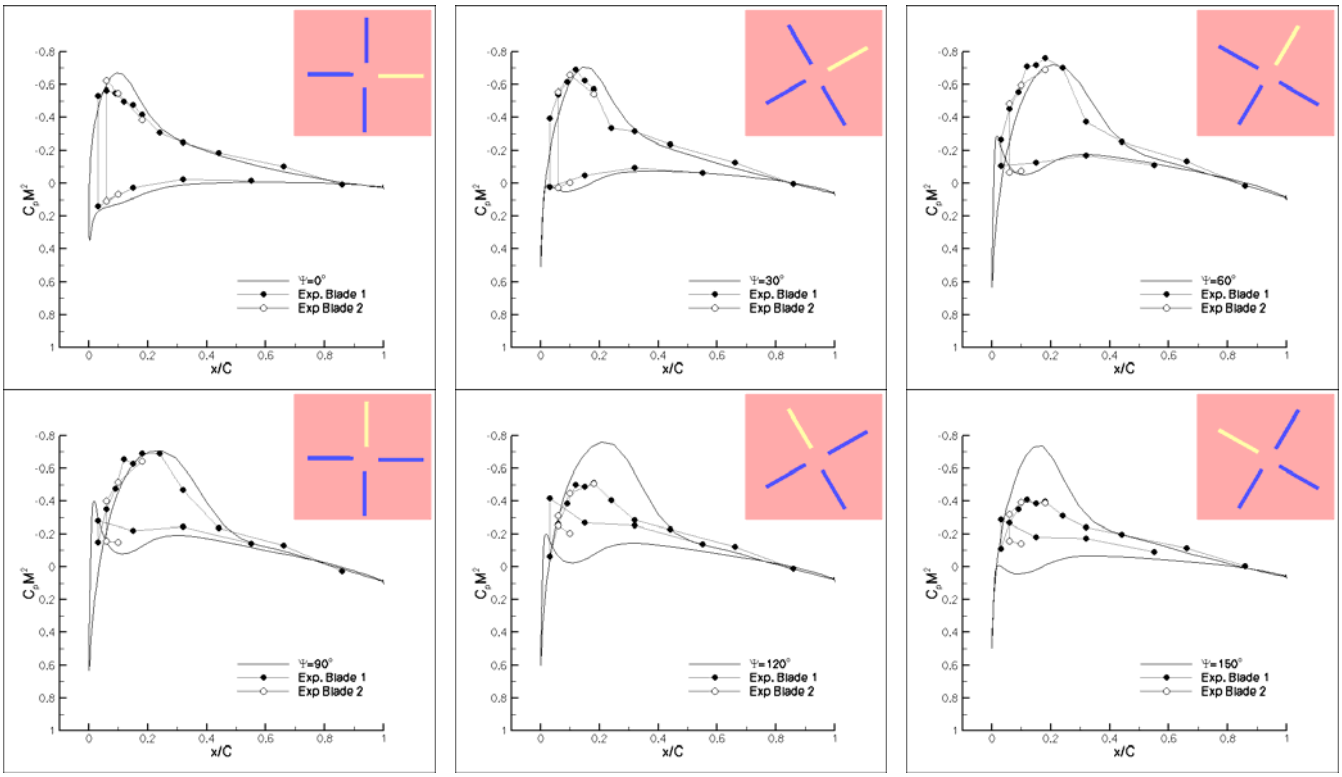

Figure 6: Comparison of computed (solid lines) and measured (symbols) unsteady pressures on the main rotor at r/R=0.87. Black and white symbols belong to different blades

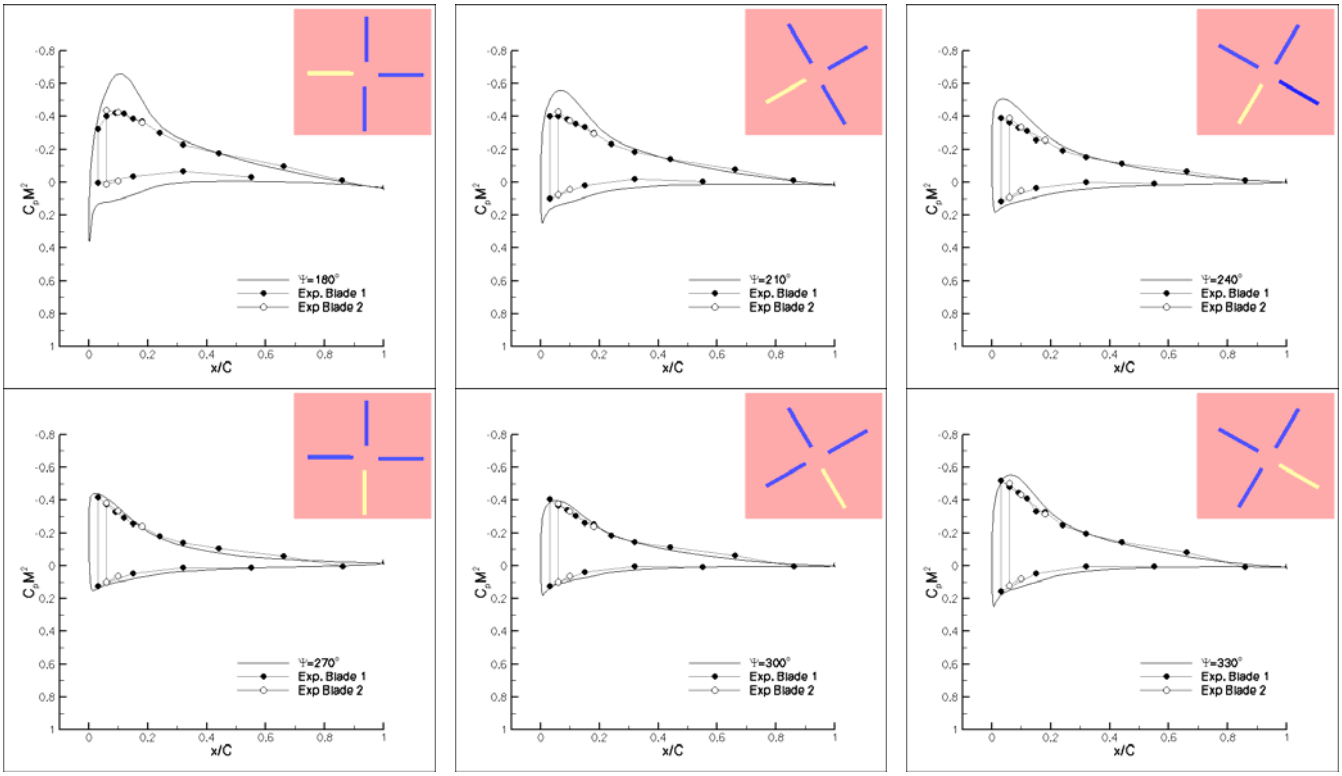

Figure 6 Continued

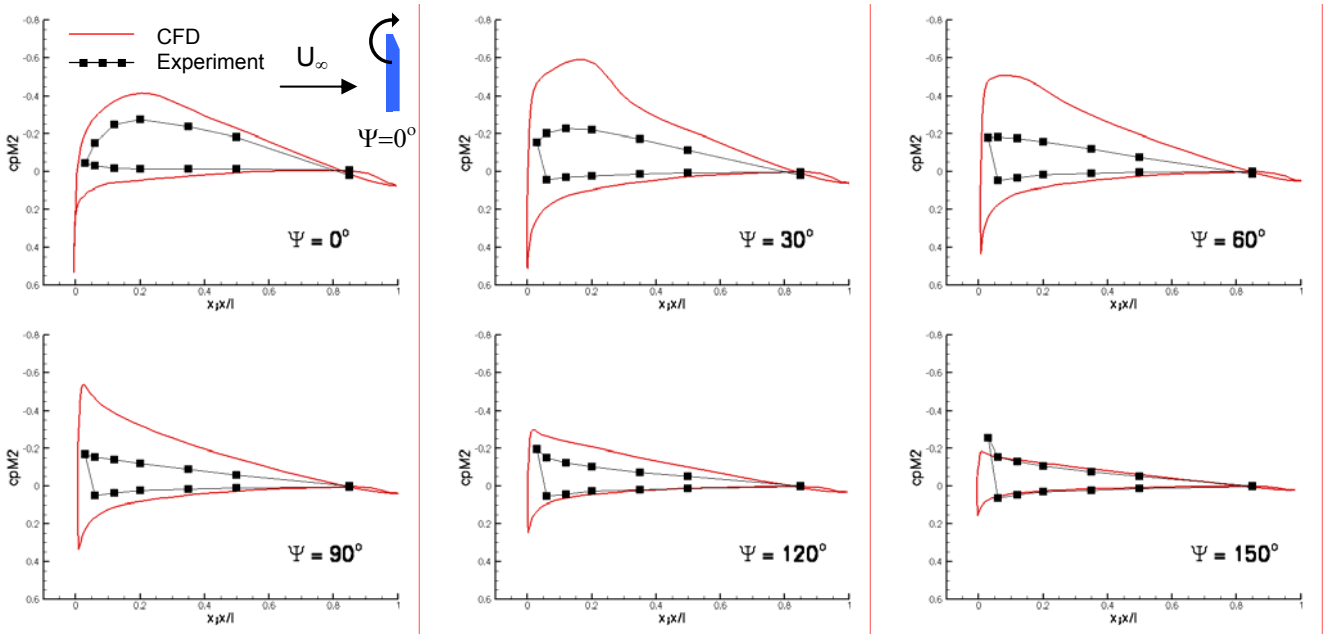

Figure 7: Comparison of computed (solid lines) and measured (symbols) instantaneous tail rotor pressures at r/R=0.80

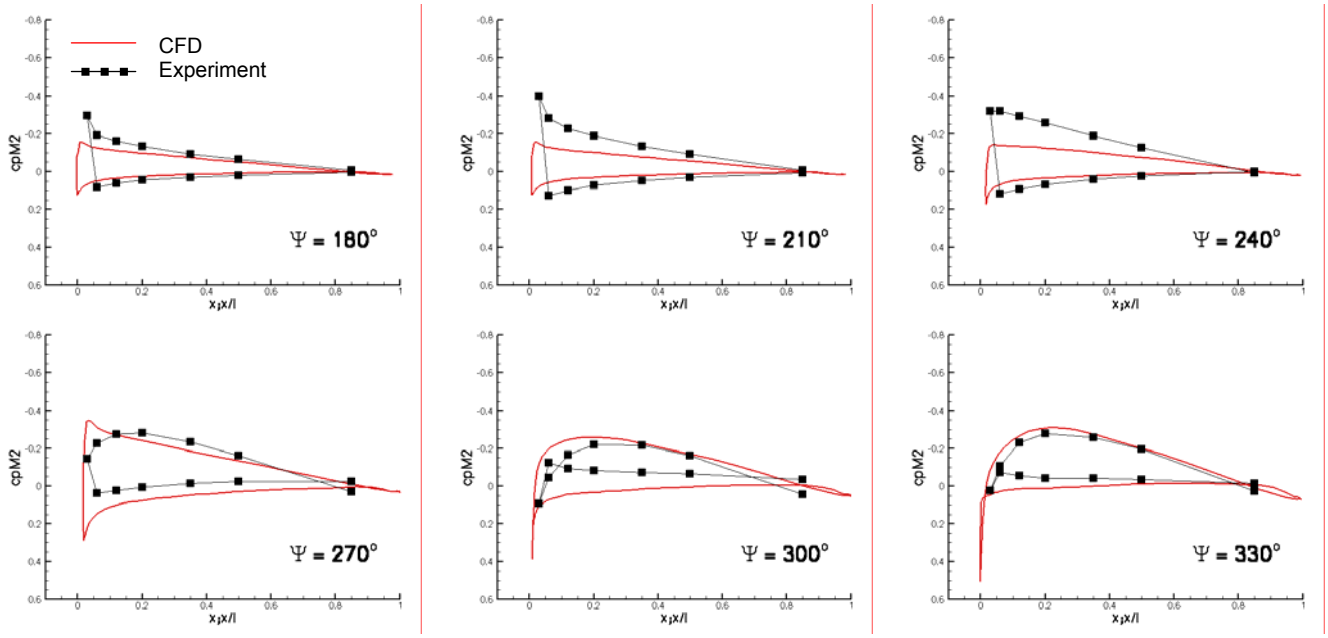

Figure 6 Continued

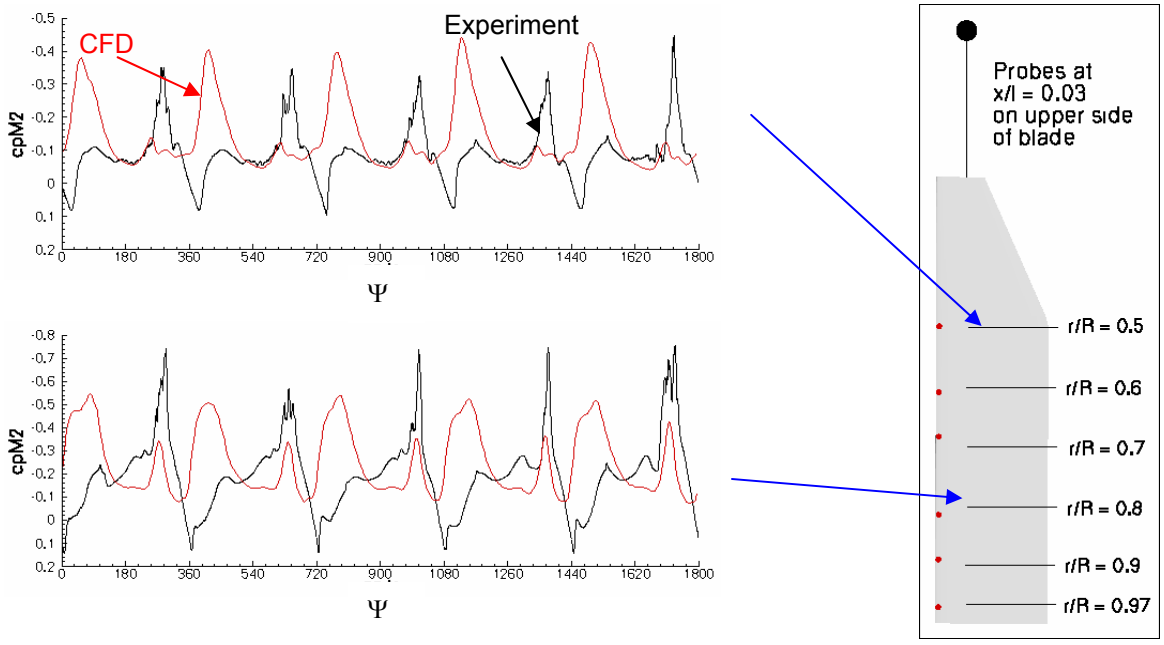

Figure 8: Variation of tail rotor pressures at r/R=0.5 and 0.8 over five tail rotor revolutions. Red curves:numerical results, Black curves:measurements